# Chapter IV

# DESIGN AND MODIFICATION OF THE IMPACTOR, PERFORMANCE TEST AND VALIDATION OF DEVELOPMENT TECHNIQUE

In this chapter, describes about the modifications of the cascade impactor and the associated experiments to test the performance of the developed technique on radon and thoron. Parameters that might affect sensitivity and reliability of the technique have been evaluated. The findings of experiments with modified cascade impactor are also reported to obtain the most desirable results.

## 4.1 Impactor design

A portable air sampler for this study has been designed to measure particulate matter (PM) exposure studies due to its sharp cut-point diameter characteristic. The design of a portable impactor is expected to be able to handle the size distribution of aerosols which would be represented by log-normal size distribution mode. A four fractionating size-selective impactor has been selected on the basis of deposition and retention of aerosol from the human respiratory tract. For most people during breathing air enters respiratory tract and aerosol particles are deposited in various regions of the human lung; extratrathoracic region (inhalable aerosol: 10-2.5 μm), tracheobronchial region (thoracic aerosol; 2.5-1 μm) and alveolar region (respirable aerosol; 1-0.5 μm). It operates in conjunction with a small, battery-operated mini-pump (MP-Σ500, SIBATA, Japan). It is a made-to-order impactor from Tokyo Dylec Corp, which manufactures several types of particle size instruments in Japan. A cross-section view of the portable cascade impactor is shown in Figure 4-1. The four nozzle array was selected to collect radon and thoron progeny on detection channel of impaction plates. The nozzles for each stage were determined by the manufacture using the Reynolds number. Marple and Liu [62] recommended a Reynold number from 300 to 3000. Moreover, the nozzle plate plays the most important role among the impactor components in terms of determining the particle collection efficiency. The number of nozzles (N) and the nozzle diameter (W) are major design parameters in a multi-nozzle impactor as reported by Marple and Willeke [63]. In this studies, we

have used four nozzle-plate and impactor plate-section for aerodynamic cut-off sizes 0.5, 1.0, 2.5 and 10 μm at a flow rate Q = 4 L $min^{-1}$. The initial (approximate) design parameters included the selection of the jet width and number to give the Reynolds number (Re) through the nozzle. The final design parameters presented in Table 4-1 were calculated assuming the following physical properties: temperature T=20 °C; pressure P=101.3 kPa; density of aerosol particles $\rho_p$=1 g $cm^{-3}$; density of air $\rho$=1.205 x $10^{-3}$ g $cm^{-3}$; and dynamic viscosity of air $\mu$=1.82 x $10^{-4}$ g $cm^{-1}$ $s^{-1}$. The impactor $d_{50}$ values were calculated using the relationship, defined as follows:

$$d_{50} \cong \sqrt{\frac{9\pi n\mu W^3 S_{tk50}}{4\rho_p QC}} \tag{4-1}$$

where the square root of the Stokes number $\sqrt{S_{tk50}}$ = 0.54 and Cunningham slip correction factor $C$ was approximated using the following equation [64].

$$C \cong 1.00 + \frac{0.16\times10^{-4}}{d_{50}} \tag{4-2}$$

Table 4-1 Design parameters for portable cascade impactor

| Parameter | Symbol (units) | Design | | | |
|---|---|---|---|---|---|
| | | Stage 1 | Stage 2 | Stage 3 | Stage 4 |
| Particle diameter at 50% impactor collection efficiency | $d_{50}$(μm) | 10 | 2.5 | 1 | 0.5 |
| Square root Stokes number at 50% collection efficiency | $\sqrt{S_{tk50}}$ | 0.54 | 0.54 | 0.54 | 0.54 |
| Reynolds number | Re | 396 | 987 | 1765 | 2657 |
| Number of impactor nozzles | n | 4 | 4 | 4 | 4 |
| Width of impactor nozzles | W(mm) | 3.59 | 1.45 | 0.81 | 0.53 |
| Jet-to-plate distance of impactor | S(mm) | 11 | 8 | 4.5 | 4 |
| Throat length of impactor nozzle | T(mm) | 5.05 | 2.05 | 1.55 | 1.50 |

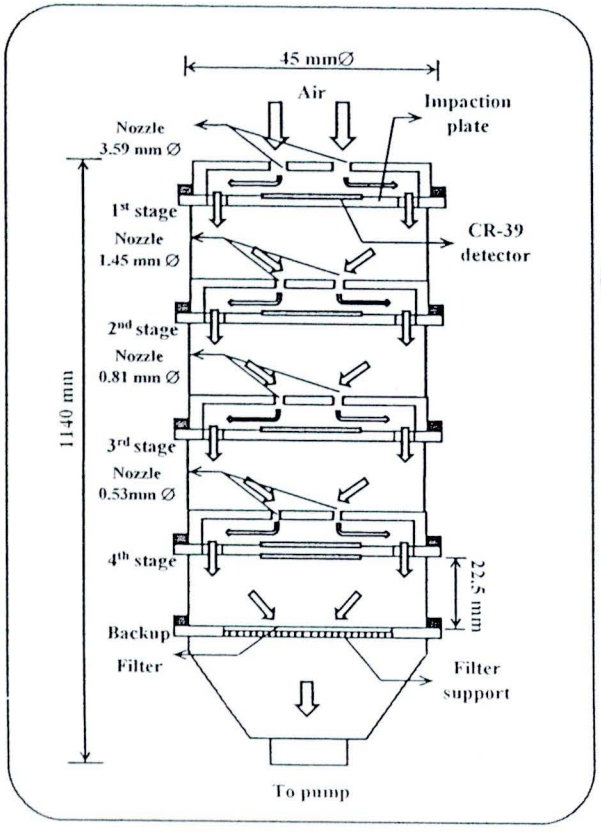




Figure 4-1 Cross-section view of portable cascade impactor.

## 4.1.1 Manufacture of portable cascade impactor

Each impactor stage consists of the identical stage wall, 4 round jets of nozzles and the impaction plate but differs in terms of nozzle diameter, and the thickness of the nozzle throat (T). This impactor is a round four-jet type with 4-size fractionating stages and a backup filter holder as shown in Figure 4-2. It is known that particles tend to focus toward the center in a straight orifice [65] which may result in their enrichment near the axis of the nozzle. Therefore, T was adjusted by modifying the thickness of the nozzle plate. In the absence of a gradual entrance region, strong aerodynamic focusing occurs which is responsible for the particle concentration enrichment that occurs in the axial region of the nozzle. To prevent an air leak from the inter-stage, O-rings were used. Fully assembled impactors were tightened in the impactor housing. In this design, aerosol particles are drawn through a series of progressively narrowing nozzles, each of which is followed by an impaction plate. After traversing the last stage (stage $4^{th}$), the stream is drawn through a backup filter

as it exits the device. Each impactor stage and a backup filter stage were tightened to prevent air leakage from the system.

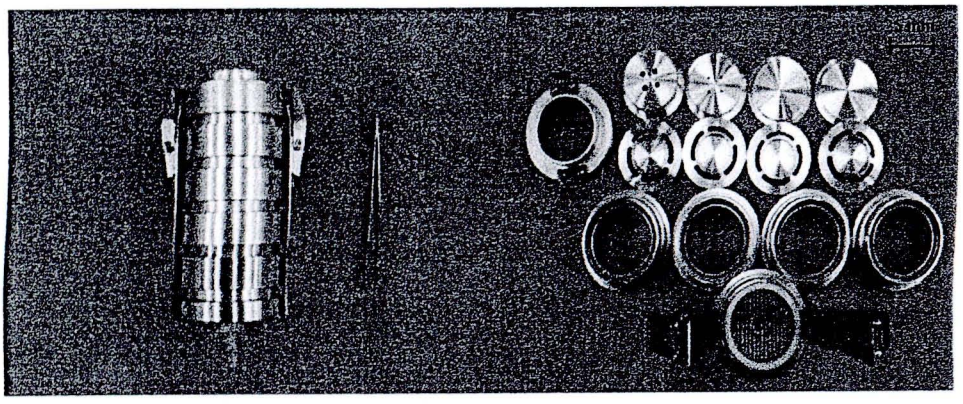

Figure 4-2 Picture of portable impactor sampler.

## 4.1.2 Modification of the collection media

In this study, the impactor has been slightly modified by inserting a CR-39 detector on the impactor plate as the collection substrate of stage 1st to 4th and on the ceiling of the backup filter holder, facing the glass microfiber filter. Figure 4-3 shows arrangement of the detection channel (CH1-CH4) on the impactor plate. In addition, each CR-39 is covered with proper aluminum vaporized Mylar films to detect the target nuclides as follows; CH1 is for $^{218}$Po, $^{214}$Po, $^{212}$Bi and $^{212}$Po, CH2 is for $^{214}$Po and $^{212}$Po, CH3 is for $^{212}$Po and CH4 is for all radionuclides. Each thickness of film is properly adjusted to let their alpha particles reach CR-39 detectors. The film thickness of each channel was evaluated in the laboratory. This technique gives information on the activity of attached radon and thoron progeny with size separation.

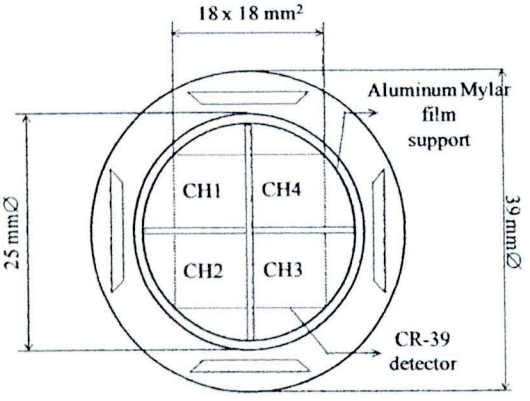


Figure 4-3 Arrangement of the detection channel on the impaction plate.

## 4.2 Performance test of impactor

In order to test the performance of impactor for radon progeny, we have used a standard radon chamber at National Institute of Radiological Sciences (NIRS). The capacity of chamber is about 25,000-L inner volume and has been shown in Figure 4-4 a). Radon concentration in the chamber was continuously monitored with an interval of 10 min by a commercially available AlphaGUARD (Genitron GmbH, Germany) ionization chamber, which was calibrated by Physikalisch Technische Bundesanstalt (PTB), Germany. Radon concentration in the chamber was maintained at about 5 kBq $m^{-3}$ in this study. For thoron progeny, a 150-L stainless steel chamber system made in NIRS as shown in Figure 4-4 b) was used. The $^{220}Rn$ concentration in the chamber was measured continuously every 1 h using a RAD7 electrostatic collection method (Durridge Co. Inc., USA) and set at about 4 kBq $m^{-3}$. The experimental set-up is shown schematically in Figure 4-5.

In order to test the influence of the detection response of the impactor on the presence of ambient aerosols, a condensation monodisperse aerosol generator Model 3472S (TSI Inc., USA) was used; aerosol particles were generated by the evaporation-condensation method and supplied into the chamber through the sampling port. Carnauba wax was used as the aerosol material in this study. The continuous particle size distribution was monitored by an ELPI, (Dekati Ltd., Finland) for the particle size bigger than 500 nm (it is operated at a flow rate of 30 L $min^{-1}$). The measured 50 % cut-off diameters for the thirteen stages were 0.029, 0.060, 0.105, 0.166, 0.255, 0.373, 0.637, 0.99, 1.61, 2.46, 3.98, 6.60 and 10.20 μm, while the aerosol particles smaller than 500 nm were measured by scanning mobility particle sizer Model 3936 (TSI Inc., USA).

The CR-39 detector was etched for 24 h at 60°C in 6.25 N NaOH solution. The etch-pits were counted by optical microscope.

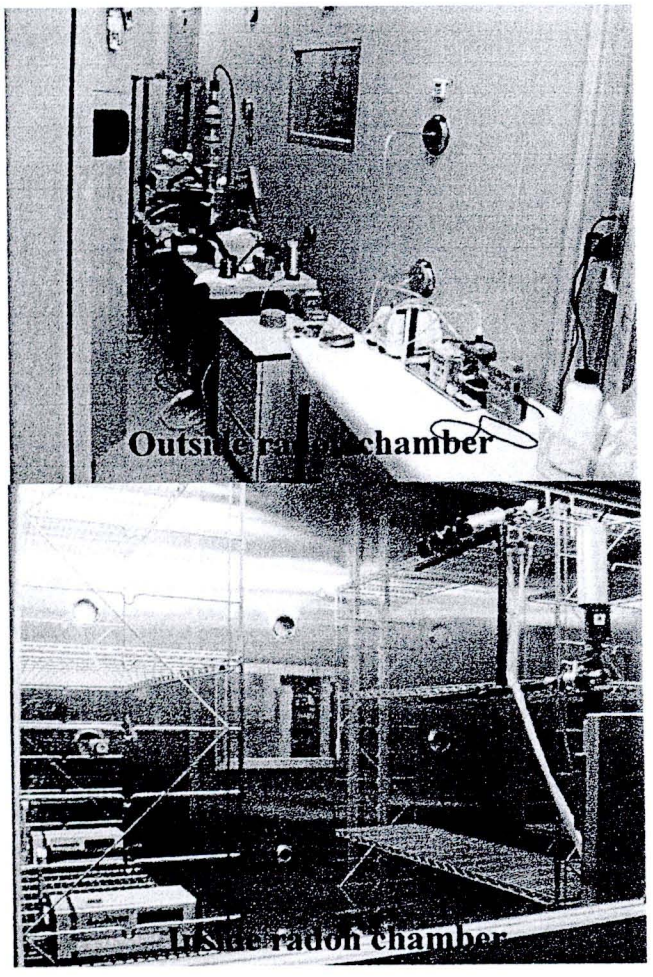


a) Radon chamber

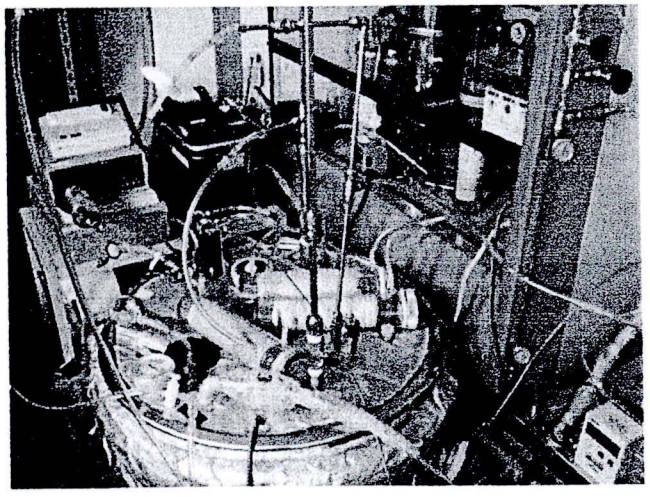

b) Thoron chamber

Figure 4-4 The illustration of reference chambers at NIRS.

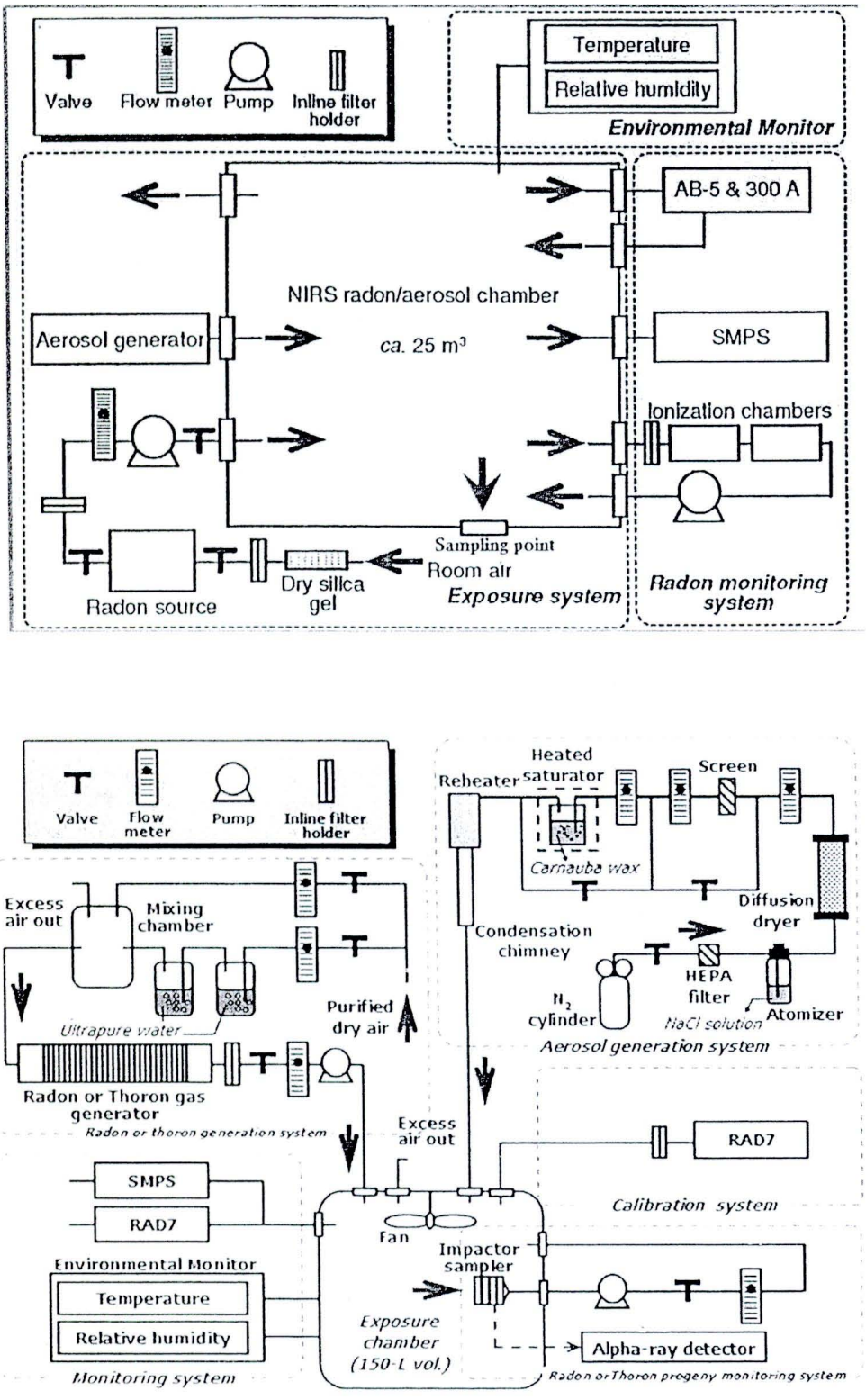


Figure 4-5 Experiment set-up for performance test: a) Radon chamber b) Thoron Chamber.

### 4.2.1 Discrimination of $^{222}Rn$ and $^{220}Rn$ progeny on CR-39 detectors with aluminum-vaporized Mylar films

In order to test the proper film area density for CH1, CH2 and CH3, the various area densities of aluminum-vaporized Mylar film corresponding to alpha particle energy of uranium-thorium and radon progeny to impinge on CR-39 were investigated. CH1, CH2 and CH3 are designed for cut-off alpha energies of about 4.2, 6.1 and 7.7 MeV from uranium-thorium, $^{218}Po$ and $^{214}Po$, respectively.

For making energy of uranium and thorium, an aluminum-vaporized Mylar film with density about 1.34 mg $cm^{-2}$ was used to attenuate $\alpha$-energy of 5 MeV to 4.2 MeV. It has been tested using a $^{241}Am$ disc source (activity 974 Bq) and can be seen in Figure 4-6 a).

Short-lived alpha source of energy 7.7 MeV with reference to $^{214}Po$ was obtained from $^{222}Rn$ progeny by taking a sample on the 47 mm glass fiber filter. Afterward, it has been attenuated to 6.1 MeV with 1.19 mg $cm^{-2}$ aluminum-vaporized Mylar film as shown in figure 4-6 b) for using as an $\alpha$-particle source.

The proper film area density for above attenuation were calculated by SRIM program [32] and carried out experiment to confirm the energy of alpha after attenuated by Alpha spectrometry system (Canberra, USA). This detector has an alpha efficiency of approximately 33% at 5.5 MeV.

In the case of proper film area density for discrimination of $^{220}Rn$ progeny from $^{222}Rn$ progeny were also calculated by SRIM program and carried out experiment to confirm the energy cutoff by CR-39.

For impactor sampler, there are two measurement geometries of alpha particles that impinge on CR-39; (A) measuring the alpha particles emitted from aerosols and impinge on CR-39 ($1^{st}$ – $4^{th}$ of impactor stages), and (B) measuring the alpha particles emitted from the surface of the glass fiber filter and impinge on the CR-39 through an air layer of 22.5 mm (back up filter holder impactor stage).

Results of triplicate measurements of the proper film area density for discrimination of $^{220}Rn$ progeny from $^{222}Rn$ progeny on CR-39 are shown in Table 4-2 and Figure 4-7.

Figure 4-8 is illustration of detector channel at each impactor plate geometry.

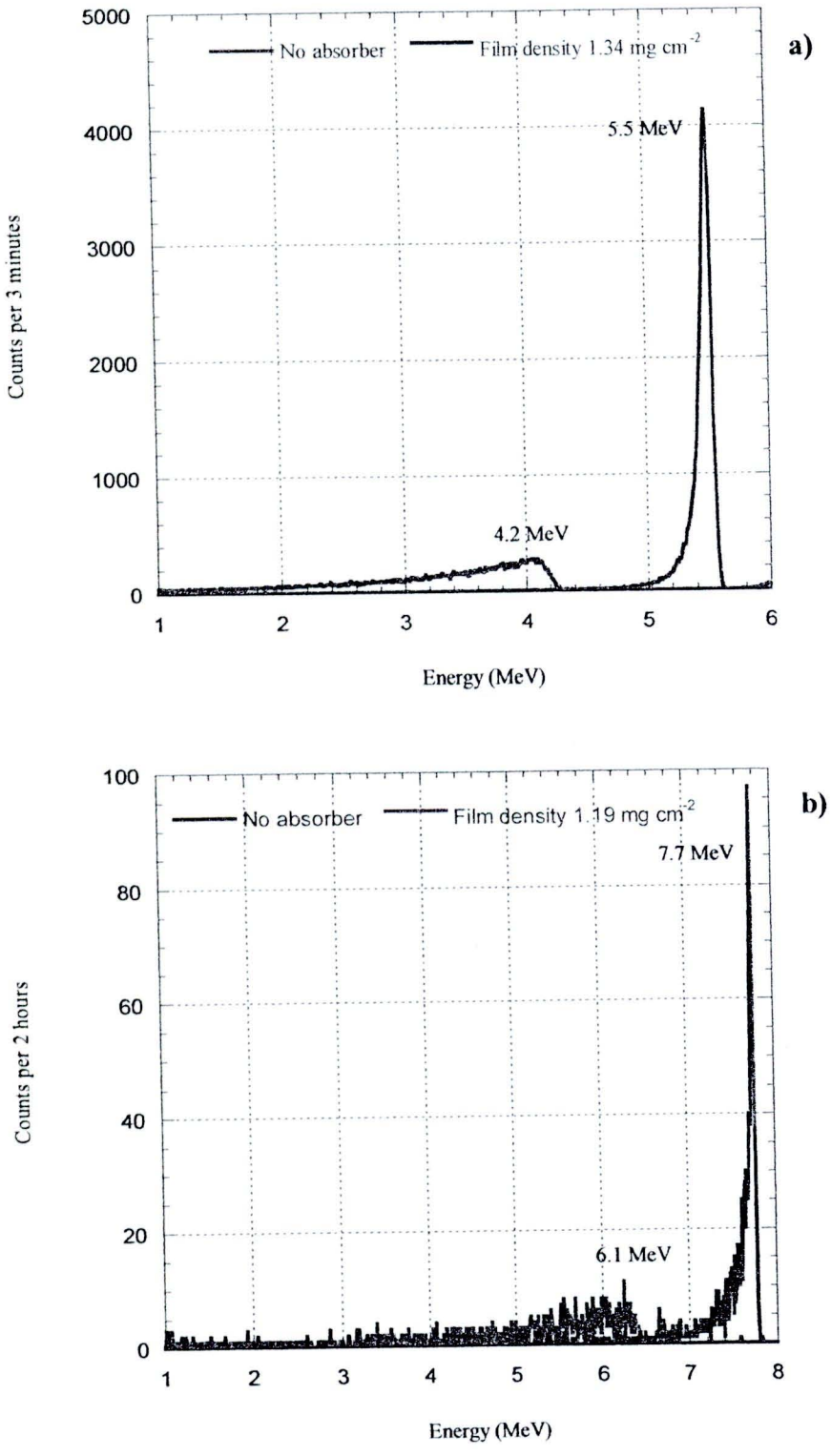


Figure 4-6 Alpha spectrum results: a) Attenuation of 5.5 MeV from Am-241 b) Attenuation of 7.7 MeV from Pb-214.

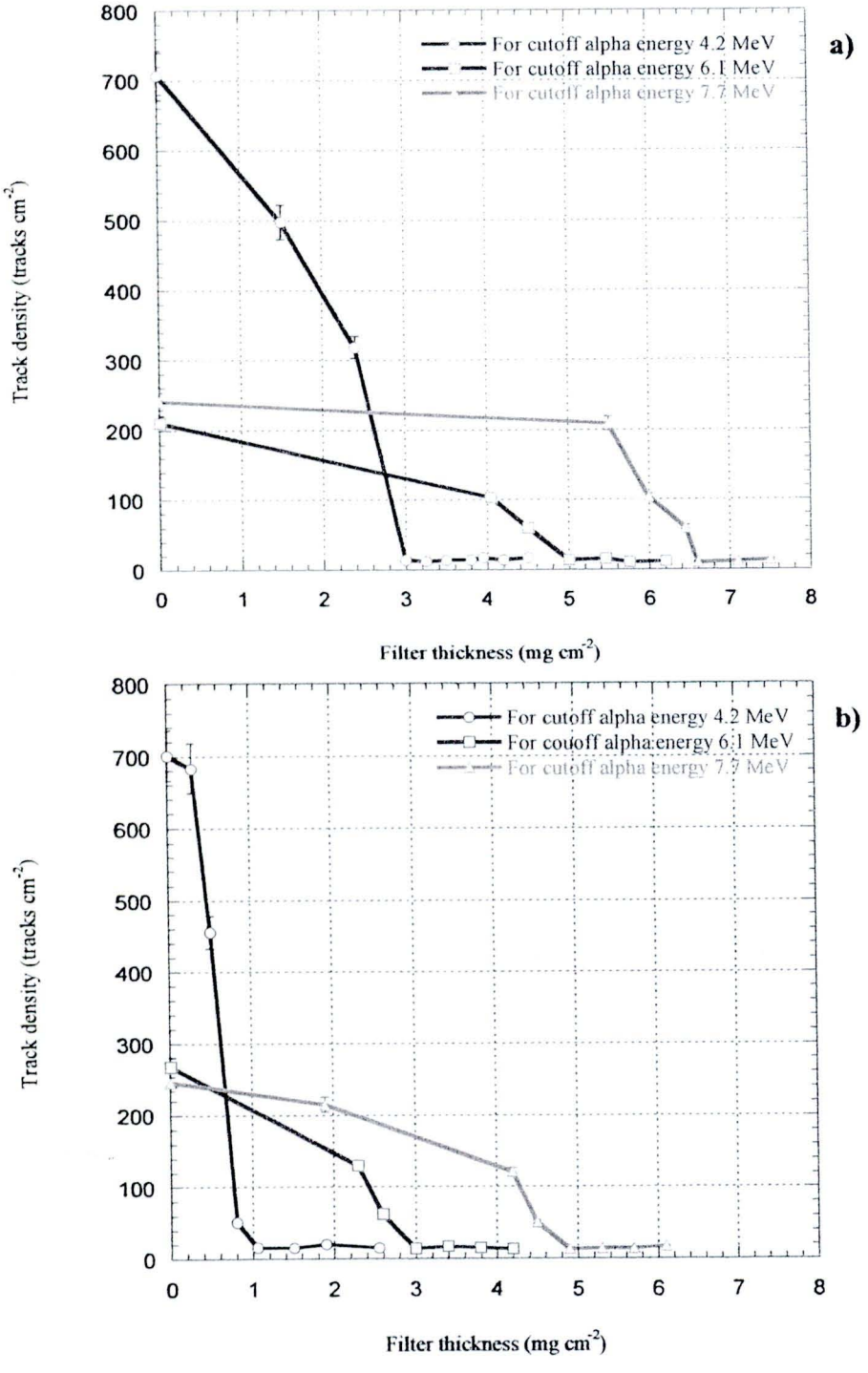


Figure 4-7 Relationship between track density and area density of film for cut-off alpha energy 4.2, 6.1 and 7.7 MeV: A) Measuring the alpha particles emitted from aerosols and impinge on CR-39. B) Measuring the alpha particles emitted from the surface of the glass fiber filter and impinges on the CR-39 through an air layer of 22.5 mm.

Table 4-2 Film area densities absorber for each channel

| Channel | Film Thickness (mg $cm^{-2}$) | | Cut-off of alpha energy (MeV) | Radionuclide collection |
|---|---|---|---|---|
| | (A) | (B) | | |
| CH1 | 3.00 | 1.05 | 4.2 | $^{218}Po$-, $^{214}Po$, $^{212}Bi$, $^{212}Po$ |
| CH2 | 5.00 | 3.00 | 6.1 | $^{214}Po$, $^{212}Po$ |
| CH3 | 7.10 | 5.00 | 7.7 | $^{212}Po$ |
| CH4 | 0.54 | 0.29 | - | Blank |

**Remark:** (A) Measuring the alpha particles emitted from aerosols and impinges on CR-39. (B) Measuring the alpha particles emitted from the surface of the glass fiber filter and impinges on the CR-39 through an air layer of 22.5 mm.

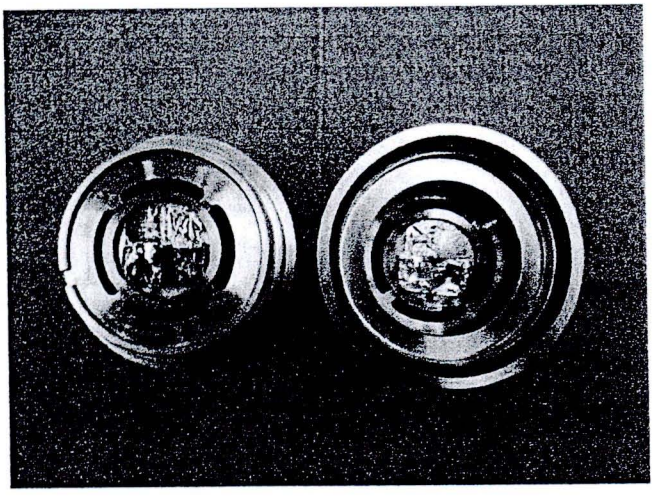

Figure 4-8 Iillustration of detector channel at each impactor plate geometry.

## 4.2.2 Detector efficiency calibration

The efficiency of this impactor is made up of two parts; (A) the counting efficiency of CR-39 at measuring the alpha particles emitted from aerosols and impinge on CR-39 through the proper aluminum-vaporized Mylar films and (B) the counting efficiency of CR-39 at measuring the alpha particles emitted from the surface of the glass fiber filter and impinge on the CR-39 through an air layer of 25 mm and the proper aluminum-vaporized Mylar films. Figure 4-9 shows the experiment for alpha-track registration in this study.

In the experiment, when evaluating counting efficiencies of alpha particles emitted from radon and thoron progeny, a part of the filter was used for alpha

registration with CR-39 detectors (size 18 x 18 $mm^2$) after air sampling. The rest was used for the alpha spectroscopic measurement to obtain an original alpha emission rate.

The collection efficiency could be calculated approximately by the following equation;

$$\eta = \frac{(N - N_{Bg})A_b \times 100}{t \times I \times A_a} \qquad (3\text{-}3)$$

Where N = alpha-track density (track $mm^{-2}$)

$N_{Bg}$ = background alpha-track density (track $mm^{-2}$)

$A_a$ = effective area of filter that used for alpha track registration ($mm^2$)

$A_b$ = effective area of a part filter that measured by alpha spectrometry ($mm^2$)

I = activity of source which measured by alpha spectrometry (Bq)

t = exposure time of track registration (s)

The value of counting efficiency is shown in Table 4-3.

Table 4-3 The average counting efficiency of CR-39

| Geometry | Counting efficiency at various film area density (%) | | Average Counting efficiency (%) |
|---|---|---|---|
| | Radon Progeny | Thoron Progeny | |
| 1. measuring the alpha particles emitted from aerosols and impinge on CR-39 through the proper Al film | 13.11 | 10.57 | 11.84 |
| 2. measuring the alpha particles emitted from the surface of the glass fiber filter and impinge on the CR-39 through an air layer of 22.5 mm and the proper Al film | 10.12 | 9.90 | 10.01 |

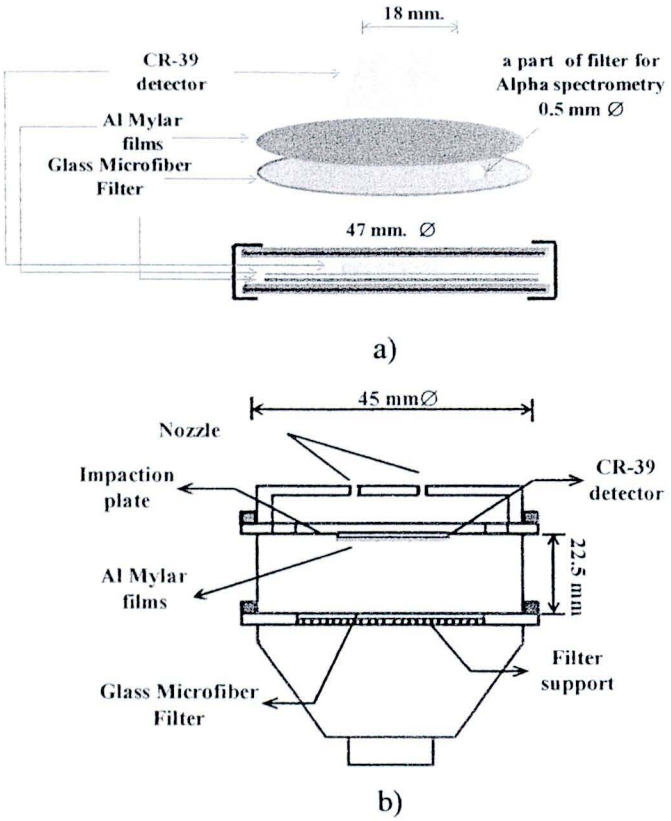


Figure 4-9 Experiment procedure for alpha track registration a) Measuring the alpha particles emitted from aerosols and impinge on CR-39. b) Measuring the alpha particles emitted from the surface of the glass fiber filter and impinges on the CR-39 through an air layer of 22.5 mm.

## 4.2.3 Impactor collection efficiency calibration

The particle collection efficiency as a function of particle size for each impactor cutpoint stages was determined using a condensation monodisperse aerosol generator (Model 3472S, TSI Inc., USA). Figure 4-10 shows a block diagram of the aerosol generator. After generation of the aerosols was mixed with room air (relative humidity: 60%, Temperature 20°C) in radon chamber (concentration 5 kBq $m^{-3}$) for 2 h. Collection efficiency was determined by measuring total activity of attached radon progeny simultaneously on a reference filter (with impactor nozzle and impactor plate) and on the filter at downstream of the impactor (without impactor nozzle and impactor plate). Sampling system for collection efficiency of attached radon progeny is shown in Figure 4-11. Attached radon progeny samples were taken through sampling port settled on the side of chamber. After 10 min sampling, alpha particles

on each filter were counted using Ludlum Scintillation Model 43-1 counters (Ludlum Measurements Inc., USA). Alpha counts were registered in 1 min increments for a period of 40 min. The counting data were analyzed by the decay method [66], yielding the Equilibrium Equivalent Radon Concentration (EERC).

In addition, the SMPS and ELPI were used to evaluate the particles in size 0.3–0.5 μm range and 0.5-10 μm range, respectively. The SMPS could not be used for particles larger than approximately 0.6 μm since they are removed by the impactor that placed in the inlet of the instrument. Each impactor stage was evaluated using the following surfaces as impaction substrates:

(a) 22.5 mm Glass fiber filter (GF/F, Whatmam)

(b) 22.5 mm Aluminum-vaporized Mylar film disk

Impaction surfaces (a) and (b) were used without any coating or adhesive material for all impactor stages.

Figure 4-12 shows the illustration of instruments which were used in this study.

The particle collection efficiency of the impactor stage ($E_C$) was calculated as

$$E_c = \frac{(C_{w/o} - C_w)}{C_{w/o}} \times 100 \qquad (3\text{-}4)$$

where $C_w$ and $C_{w/o}$ are the activity of attached radon progeny with and without the impactor nozzle and impactor plate, respectively.

The result from collection efficiencies of portable impactor stage 3$^{rd}$ (1μm) and stage 4$^{th}$ (0.5 μm) are presented in Table 4-4 and Figure 4-13 ~14. Particle collection efficiency data for each stage are plotted as a function of particle diameter. The collection efficiencies using two different materials as impaction substrates are shown in the same graph for direct comparison. The experiment data were fitted using a sigmoidal function. The cut point diameters of each impaction substrate are summarized in Table 4-5.

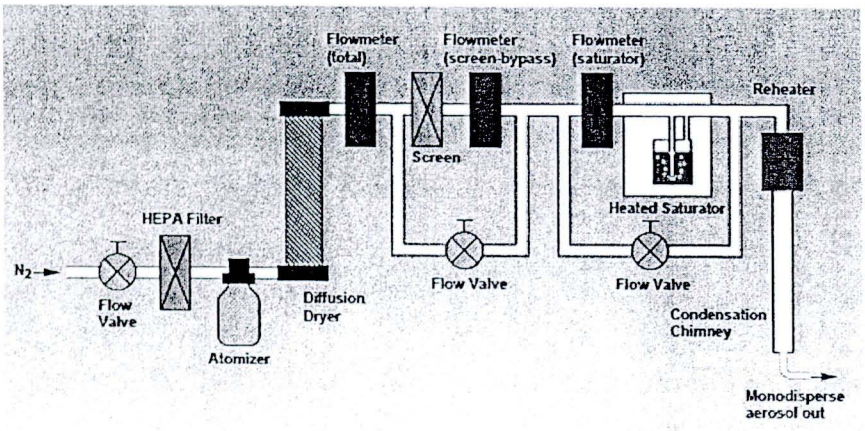


Figure 4-10 A block diagram of aerosol generator.

Table 4-4 The collection efficiency of portable impactor

| Impactor Stage | Aerosol size (μm) | $C_w$ (Bq m$^{-3}$) | | $C_{w/o}$ (Bq m$^{-3}$) | | $E_C$ (%) | |
|---|---|---|---|---|---|---|---|
| | | filter | Al disk | filter | Al disk | filter | Al disk |
| 3 | 0.546 | 1239 | 1269 | 1283 | 1274 | 3.413 | 0.39 |
| | 0.637 | 995 | 1187 | 1208 | 1269 | 17.63 | 6.46 |
| | 0.715 | 920 | 1299 | 1182 | 1502 | 22.16 | 13.52 |
| | 0.905 | 193 | 259 | 690 | 619 | 72.03 | 58.16 |
| | 1.230 | 6 | 92 | 641 | 621 | 99.06 | 85.18 |
| 4 | 0.384 | 234 | 272 | 293 | 286 | 20.14 | 4.89 |
| | 0.458 | 813 | 1120 | 1403 | 1520 | 42.05 | 25.43 |
| | 0.546 | 499 | 572 | 1265 | 1253 | 60.55 | 54.35 |
| | 0.637 | 207 | 290 | 1182 | 1501 | 82.49 | 80.67 |
| | 0.715 | 176 | 237 | 1283 | 1322 | 86.28 | 82.07 |

Table 4-5 Cut point diameters of each impaction substrate for impactor stage 3 and 4

| Stage No. | Cut-point diameter (μm)[a] | |
|---|---|---|
| | GF/F filter | aluminum vaporized Mylar films |
| 3 | 0.95±0.04 | 1.00±0.03 |
| 4 | 0.50±0.17 | 0.53±0.06 |

[a]Determined by sigmoidal function

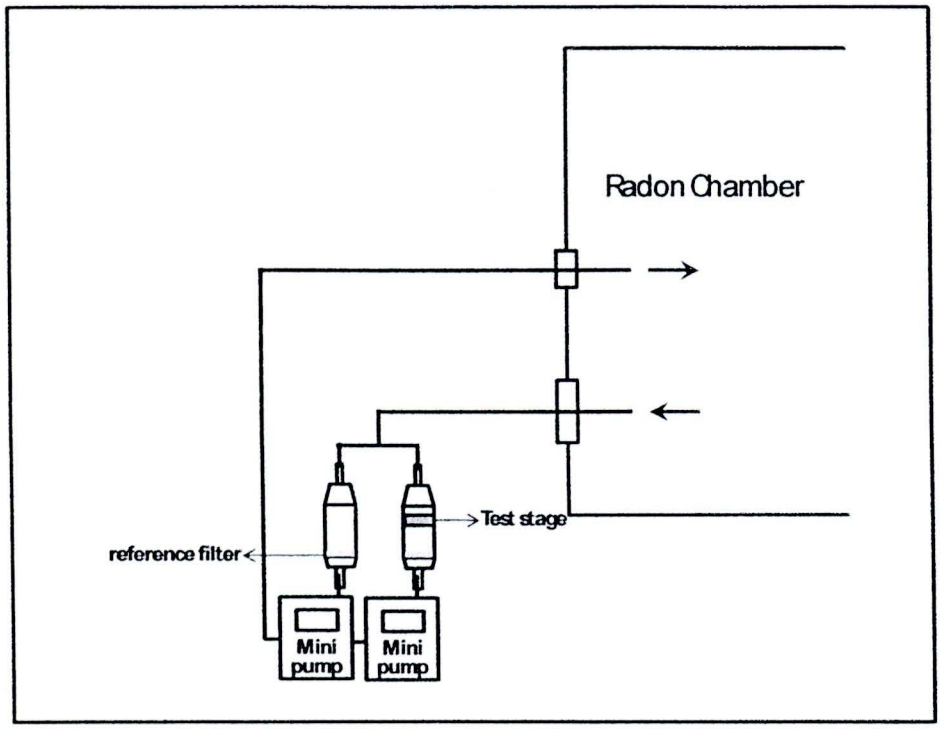


a) Sampling system block diagram

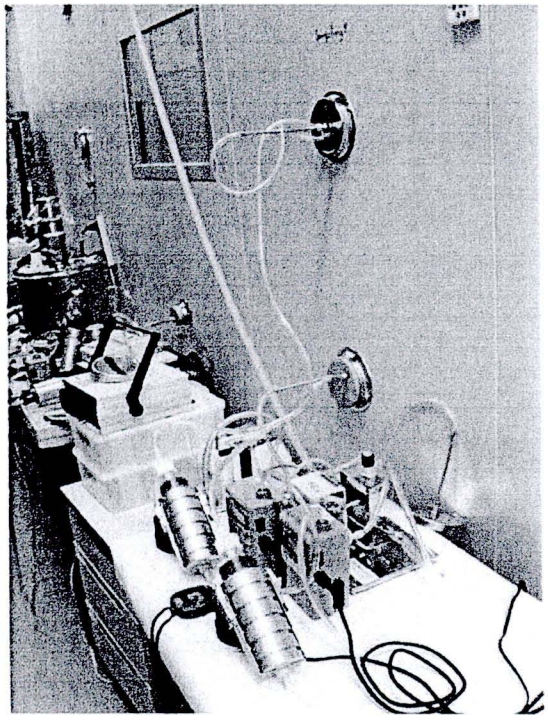

b) Illustration of sampling system

Figure 4-11 Sampling system for collection efficiency of attached radon progeny.

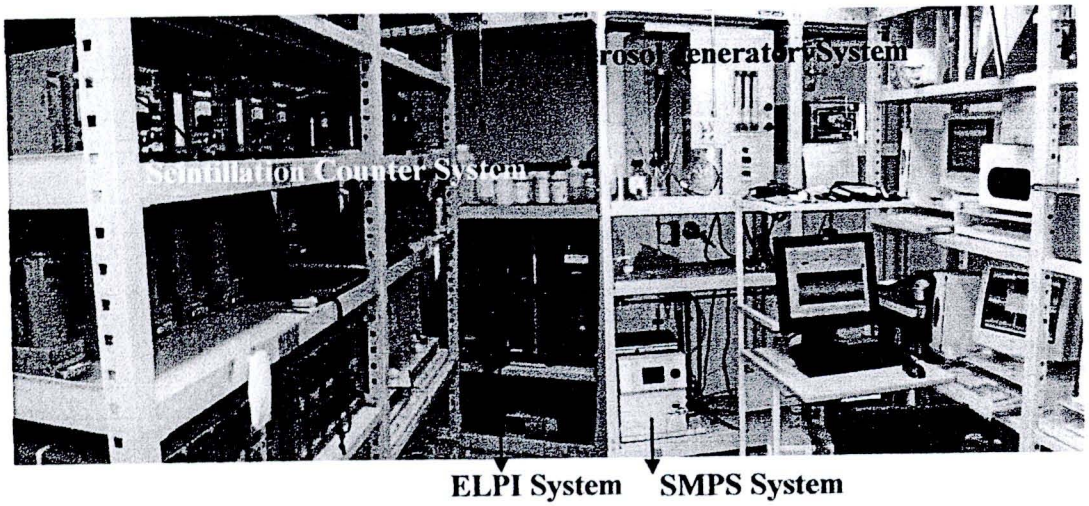


Figure 4-12 The illustration of instruments for collection efficiency calibration.

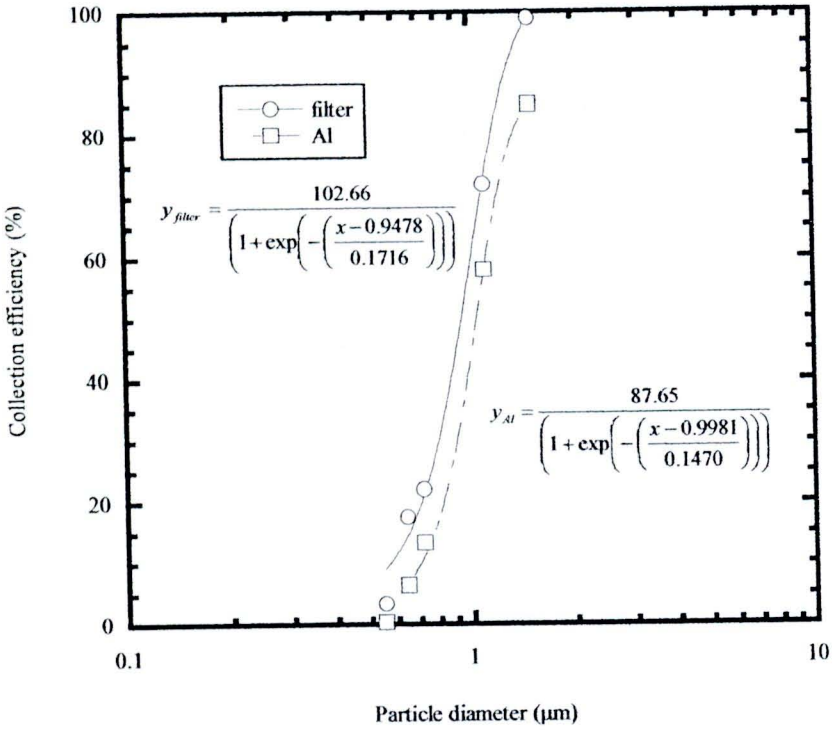


Figure 4-13 Collection efficiency of stage 3 (1 μm).

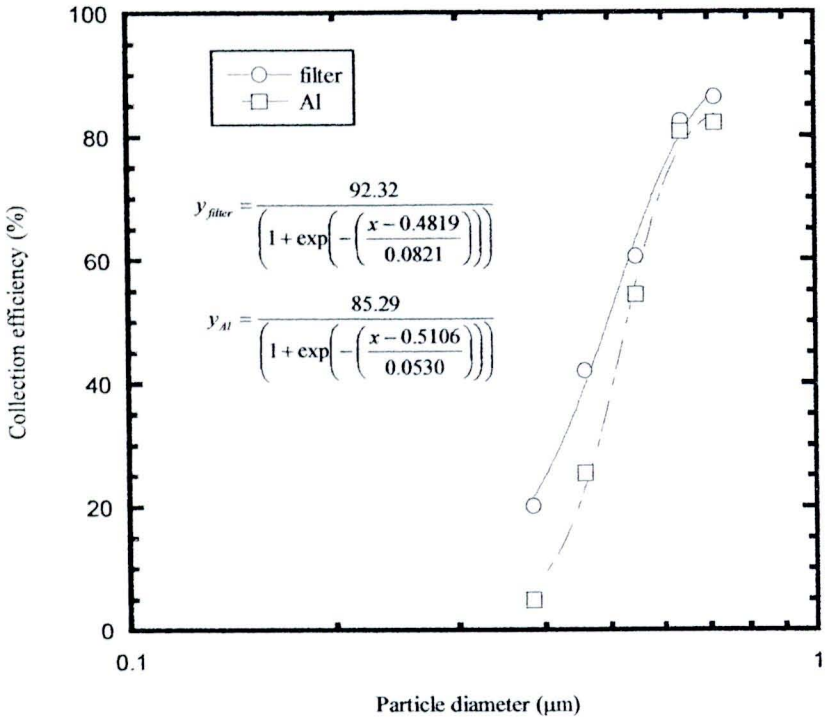


Figure 4-14 Collection efficiency of stage 4 (0.5 μm).

From the experimental collection efficiency data of stage 3 and 4 indicated that the 50% collection efficiency cut-point for filter and aluminum are closed to the design cut-point. Particle collection efficiency of aluminum substrate also decreased for particles smaller than 0.5 μm when compared with GF/F filter substrate, probably due to some particle bounce on that surface. This phenomenon is more likely to occur in the aluminum substrates because of the higher surface hardness of aluminum compared to filter paper.

The sharpness of the collection efficiency curve of an impactor can be defined in terms of the geometric standard deviation ($\sigma_g$), which is the square root of the ratio of the aerodynamic particle diameter corresponding to 16% collection efficiency to that corresponding to 84% efficiency [67]. Based on this principle, the values of σg for each stage and substrates were estimated and listed in Table 4-6.

Generally, lower $\sigma_g$ values indicate the higher precision in particle separation characteristics of a given impaction stage, which is highly desirable feature of an impactor as it leads to a finer resolution in the size distribution of an aerosol. The

value of $\sigma_g$ is approximately about 1.7–1.9 for filter and aluminum substrates, thereby indicating reasonably sharp particle separation characteristics when these two substrates were used.

Table 4-6 Sharpness of the collection efficiency for stage 3rd and 4th of the portable impactor as a function of substrate

| Impactor stage (cut point diameter; μm) | Substrate type | $\sigma_g$ |
|---|---|---|
| 3 (1) | filter | 1.37 |
| | Al | 1.37 |
| 4 (0.5) | filter | 1.38 |
| | Al | 1.30 |

Unfortunately, we could not check the cut point diameter of stage 1st (10 μm) and stage 2nd due to limitation of aerosol generation system at NIRS which could not generated aerosol size bigger than 1.3 μm.

Taking into consideration of all the above experimental conditions, it could be assumed that the 50% collection efficiency cut-point for stage 1st and 2nd are also closed to the design cut-point of 10 and 2.5 μm, respectively.

## 4.3 Evaluation parameter that might affect the sensitivity of developed technique

In order to evaluate parameter that might affect sensitivity of the developed technique, radon chamber of NIRS was used. The radon concentration was maintained at about 5 kBq $m^{-3}$. For ambient aerosols, a condensation monodisperse aerosol generator Model 3472S was used; aerosol particles were generated by the evaporation-condensation method and supplied into the chamber through the sampling port. Carnauba wax was used as the aerosol material to generate a targeted aerosol size around 0.3 - 1 μm. The ambient aerosol concentration depends on the particle size and became constant 2 h after aerosol particles were injected into the chamber. The continuous particle size distribution was monitored by an ELPI. The developed technique was used for size measurement. The sampling and measuring time were 5 min and 4 h, respectively.

The CR-39 detectors were etched for 24 hours at 60° C in 6.25 N NaOH solution. The etch-pits were counted by a microscope. The Equilibrium Equivalent Radon concentration (EERC) and Equilibrium Equivalent Thoron concentration (EETC) were calculated theoretically from the etch-pit counts on the CR-39 detector that divided in to four channels by the equations 3.5 and 3.6, respectively.

The example of etch pit on the surface of CR-39 at each detection channel were shown in Figure 4-15.

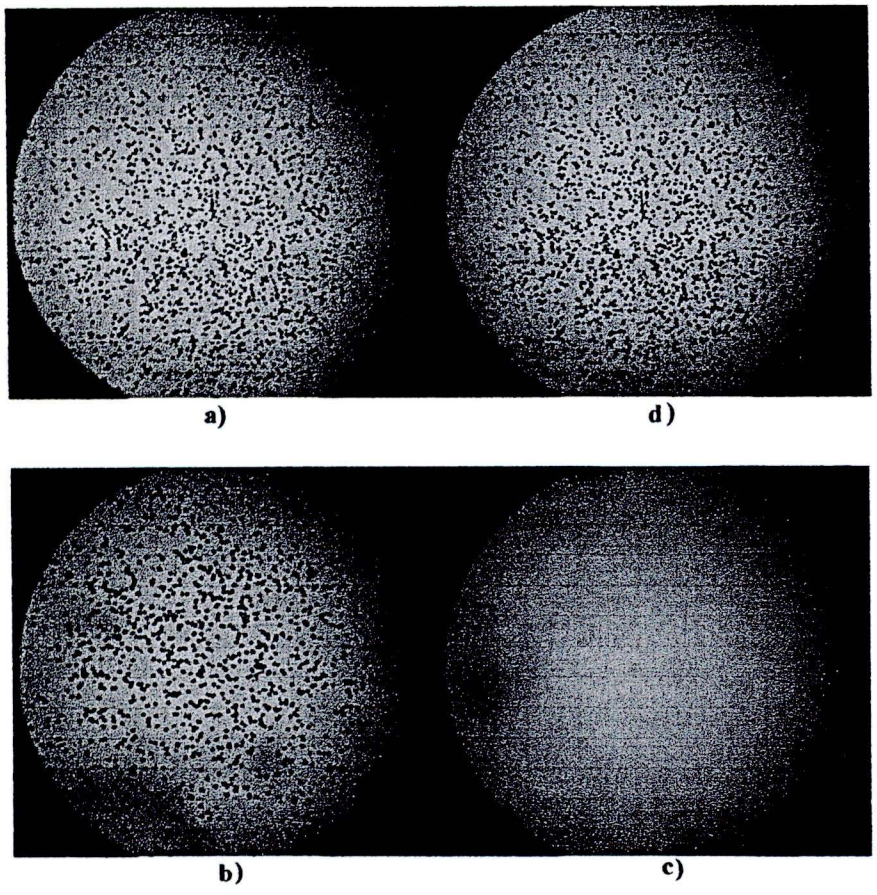


Figure 4-15 The illustration of etch pits on the surface of CR-39 at each detection channel of stage 3rd (Magnification: 100×). Sampling at radon concentration 5 $kBqm^{-3}$ and aerosol size 1 μm was generated: a) CH1, b) CH2, c) CH3 and d) CH4.

**Calculation method of EERC and EETC for portable impactor**

For radiation protection purposes, the potential alpha energy concentration (PAEC) is usually the quantity of interest and it often measured in unit of Working

Level (WL). Another quantity of interest is the equilibrium equivalent concentration (EEC) measured in units of activity per unit volume.

A working level, WL, was originally defined as any combination of short-lived radon progeny ($^{218}$Po, $^{214}$Pb, $^{214}$Bi, $^{214}$Po), and later by extension any combination of short-lived thoron progeny ($^{216}$Po, $^{214}$Pb, $^{212}$Bi, $^{212}$Po), in 1 liter of air at normal temperature and pressure that had the potential to release $1.3 \times 10^5$ MeV of alpha particle energy in their ultimate radioactive decay.

The potential alpha energy concentration in air, is the sum of the potential alpha particle energy of all the short-lived radon or thoron progeny in a unit volume of air. The unit of potential alpha energy concentration defined as J $m^{-3}$ or MeV $m^{-3}$.

The equilibrium-equivalent concentration, EEC, of a non-equilibrium mixture of radon or thoron progeny is the activity concentration of the parent radon or thoron gas in equilibrium with its short-lived progeny that has the same potential alpha energy concentration as the actual non-equilibrium mixture.

Therefore, EERC and EETC are theoretically calculated by the equation as follows;

$$EERC = \frac{\left(E_{Po-218} \times N_{Po-218\,inCH1}\right) + \left(\left(E_{Po-214} - E_{Po-218}\right) \times N_{Po-214\,in\,CH2}\right)}{\eta \times T \times V} \times 2.846 \times 10^{-5} \quad (4\text{-}5)$$

$$EETC = \frac{\left[\left(E_{Bi-212} \times 0.561\right) + E_{Po-212}\right] \times N_{CH3}}{\eta \times T \times V} \times 0.215 \times 10^{-5} \quad (4\text{-}6)$$

where the counts of etch-pits on all channels are obtained with $E_i$, $N_{i\text{-}ch}$, $T$, $V$, and $\eta$.

$E_i$ is alpha energy of $i$-nuclide in (MeV),

$N_{i\text{-}ch}$ is number of alpha tracks due to $i$-nuclide in the detection area of $i$-channel,

$T$ is collecting period in (min),

$V$ is flow rate in ($m^3$ $min^{-1}$),

$\eta$ is the CR-39 collection efficiency,

The collection efficiency was estimated deriving from the experiment and found 2.846 x $10^{-5}$ and 0.215 x $10^{-5}$ (Bqm-$^3$ (MeV $m^{-3}$)$^{-1}$) as the conversion constant for calculation of EERC and EETC from PAEC of radon and thoron progeny, respectively.

$N_{\text{Po-218 in CH1}}$ and $N_{\text{Po-214 in CH2}}$ are obtained by the following equations 3-7 and 3-8, respectively;

$$N_{Po-218\ in\ CH1} = N_{CH1} - \left(\frac{1}{0.6406}\right) N_{CH3} \tag{4-7}$$

$$N_{Po-214\ in\ CH2} = N_{CH2} - N_{CH3} \tag{4-8}$$

where $N_{\text{CH1}}$, $N_{\text{CH2}}$ and $N_{\text{CH3}}$ mean the alpha track count on CH1, CH2 and CH3, respectively. Therefore, $N_{\text{Po-218 in CH1}}$ and $N_{\text{Po-214 in CH2}}$ are counts per unit area of alpha track by $^{218}$Po + $^{214}$Po and $^{214}$Po only, respectively.

The particle size distributions were described in terms of a log-normal distribution, defined by the activity median aerodynamic diameter (AMAD) and geometric standard deviation ($\sigma_g$). In addition to this numerical evaluation, the impactor data were also evaluated by a graphical method (Cumulative method) [64].

**Detection limit**

Detection limits in a measurement process can be explained as an analytical process leads to a quantitative detection and decides the results of analysis between a radioactive or non-radioactive. This is particularly relevant when the sample counts are very close to background and accurate measurements of sample counts and background counts must be made to distinguish the difference within reasonable error limits. The longer the counting time, the lower is detection level or minimal detectable activity (MDA). The MDA also referred to as the lower limits of detection (LLD) in Bq m$^{-3}$ that yields a net count of above background with a 95% probability. In this case, LLD [68] can be expressed as:

$$LLD = \frac{2.706}{t} + 4.653\sqrt{\frac{R_{bg}}{t}} \tag{4-9}$$

where $t$ is collecting period in (min),

$R_{bg}$ is the number of background alpha tracks on CR-39,

$LLD$ is the lower limit of detection in track count.

The $LLD$ can be converted to activity through the detector efficiency factor and a measured volume. Therefore, the LLD for EERC and EETC ($LLD_{RnP}$ and $LLD_{TnP}$ in Bq m$^{-3}$) are calculated by the following questions:

$$LLD_{RnP} = 0.09 V_{total}^{-1} \quad (4\text{-}10)$$

$$LLD_{TnP} = 0.01 V_{total}^{-1} \quad (4\text{-}11)$$

Where $V_{total}$ is the total air volume passing through the impactor in ($m^3$),

For a period of 6 h continuous sampling 4 L $min^{-1}$, we have obtained 0.13 Bq $m^{-3}$ and 0.02 Bq $m^{-3}$ for EERC and EETC, respectively. The LLD will improve with longer sampling.

## 4.3.1 Humidity

In order to investigate the effect of humidity on the developed technique, the following environmental parameters in the radon chamber were set: temperature at 20°C and at different relative humidity e.g. 20, 60 and 90%. Two to three air samples were taken under each of environment conditions.

The data obtained in this experiment is shown in Table 4-7.

In this study, the influence of relative humidity on activity median aerodynamic diameter (AMAD) of particle size 0.3 and 1 μm using the developed technique was investigated. It was found that relative humidity had no effect on AMAD of particle size 0.3 and 1 μm using the developed technique. The aerosol material in this study was carnauba wax, which is insoluble in water. On the other hand, the size effect can be found, while increasing of relative humidity on fine salt aerosols such as NaCl, $Na_2SO_4$ and $NaNO_3$ [69].

Table 4-7 AMAD and $\sigma_g$ at various relative humidity

| Aerosol condition | Relative humidity (%) | AMAD(μm) | $\sigma_g$ | Average AMAD (μm) |
|---|---|---|---|---|
| 0.3 μm | 30 | 0.433 | 2.08 | 0.431±0.003 |
| | | 0.429 | 1.89 | |
| | 60 | 0.417 | 2.63 | 0.429±0.016 |
| | | 0.440 | 1.91 | |
| | 90 | 0.383 | 2.94 | 0.415±0.045 |
| | | 0.446 | 1.92 | |
| 1 μm | 30 | 1.037 | 1.94 | 1.127±0.121 |
| | | 1.264 | 1.92 | |
| | | 1.079 | 1.78 | |
| | 60 | 1.129 | 1.97 | 1.100±0.028 |
| | | 1.099 | 2.07 | |
| | | 1.073 | 1.81 | |
| | 90 | 1.100 | 2.06 | 1.075±0.099 |
| | | 1.159 | 1.99 | |
| | | 0.966 | 1.97 | |

## 4.3.2 Temperature

In order to investigate the effect of temperature on the developed technique, the following environmental parameters in the radon chamber were set at 60 % relative humidity and temperature set at 10°C, 20°C and 30 °C. Two air samples were taken under each of environment conditions.

The data obtained in this experiment is shown in Table 4-8.

Table 4-8 AMAD and $\sigma_g$ at various temperatures

| Aerosol condition | Temperature °C | AMAD (μm) | $\sigma_g$ | Average AMAD (μm) |
|---|---|---|---|---|
| 1 μm | 10 | 0.983 | 2.21 | 0.960±0.030 |
| | | 0.971 | 1.88 | |
| | | 0.926 | 1.94 | |
| | 20 | 0.989 | 2.32 | 0.944±0.040 |
| | | 0.913 | 1.86 | |
| | | 0.931 | 2.19 | |
| | 30 | 1.111 | 2.34 | 1.022±0.087 |
| | | 0.937 | 1.81 | |
| | | 1.017 | 1.84 | |

In this study, the influence of temperature on activity median aerodynamic diameter (AMAD) of particle size 1 μm using the developed technique was investigated. It was found that temperature had no effect on AMAD of particle size 1 μm. The aerosol material in this study was carnauba wax which melts at 80°C.

## 4.3.3 Unattached progeny

In order to investigate the effect of unattached progeny on the developed technique, with and without a 400-mesh metal wire screen (TETKO Inc., USA) was set at the top of the impacter sampler. The 400-mesh wire screen can prevent invasion of unattached progeny (1 - 10 nm) by diffusion with collection efficiency about 99.9%, while minimizing the collection by impaction and interception of attached progeny (0.1 – 10 μm) to less than 5%. These based on fan model filtration theory. Three different unattached fractions were tested. Table 4-9 shows experimental results for the effect of unattached progeny.

Table 4-9 Experimental results for the effect of unattached progeny

| Test ID | Unattached fraction ($f_u$) | Track density (tracks/mm$^2$) | | | | | | | |
|---|---|---|---|---|---|---|---|---|---|
| | | Stage 1 | | Stage 2 | | Stage 3 | | Stage 4 | |
| | | W | WO | W | WO | W | WO | W | WO |
| 1 | 0.010 | 0.02±0.01 | 0.02±0.01 | 0.03±0.01 | 0.04±0.01 | 0.18±0.03 | 0.17±0.03 | 6.70±0.16 | 7.04±0.17 |
| 2 | 0.041 | 0.02±0.01 | 0.05±0.01 | 0.12±0.02 | 0.18±0.03 | 7.44±0.17 | 7.05±0.16 | 0.64±0.05 | 0.53±0.05 |
| 3 | 0.107 | 0.03±0.01 | 0.11±0.02 | 0.03±0.01 | 0.08±0.02 | 0.19±0.03 | 0.20±0.03 | 0.65±0.05 | 0.68±0.05 |

W =with 400-mesh wire screen
WO=without 400-mesh wire screen

The track density in test ID2 and 3 were observed higher about 2.5 and 3.7 times for stage 1 and 1.5 and 2.7 times for stage 2, respectively on unused the 400-mesh wire screen. This is due to the unattached radon progeny deposited on the CR-39 surface. To reduce this effect, the 400-mesh wire screen should be used in the sampling system of impactor sampler.

## 4.3.4 Changing of air sampling flow rate

In order to investigate the effect of air flow rate change on the developed technique, six different airflow rates were tested (1, 2, 3, 3.5, 4, and 4.5 Lm$^{-1}$). One or Two air samples were taken under each of airflow rate. Table 4-10 shows experimental results for the effect of airflow rate change.

In this study, the influence of airflow rate on activity median aerodynamic diameter (AMAD) of particle size 1 μm was investigated. It shows that the airflow rate change about 50-75% had more effect on AMAD about 20-40%. This effect due to the particle cut off diameters of each stage was changed according to airflow rate change. In the case of airflow rate change from 4 to 1 Lm$^{-1}$, the cut off diameter of stage 1$^{st}$ to 4$^{th}$ were calculated and found that it changed to 20, 5, 2 and 1 μm, respectively.

Table 4-10 Experimental results for the effect of airflow rate change

| Aerosol condition | Airflow rate (Lm$^{-1}$) | AMAD (μm) | $\sigma_g$ | Average AMAD (μm) |
|---|---|---|---|---|
| 1 μm | 1 | 0.611 | 2.30 | 0.611 |
| | 2 | 1.284 | 2.19 | 1.284 |
| | 3 | 1.094 | 2.25 | 1.108±0.019 |
| | | 1.121 | 2.22 | |
| | 3.5 | 1.031 | 2.32 | 1.097±0.093 |
| | | 1.163 | 2.10 | |
| | 4* | 1.046 | 2.01 | 1.042±0.006 |
| | | 1.037 | 1.94 | |
| | 4.5 | 0.980 | 2.08 | 1.089±0.156 |
| | | 1.197 | 2.17 | |

* The proper airflow rate for portable impactor in this study.

## 4.4 Validation of developed technique

The AMAD of attached radon progeny in this study was verified using ELPI and MOUDI. Three aerosol particles with peak diameter of 0.3, 0.5 and 1 μm were tested.

In this study, the impactor sampler and measuring technique described earlier. It was operated at a flow rate of 4 $Lmin^{-1}$ for a period of 5 min. After sampling, it was left for 4 hour to allow all $^{214}Bi$ decay to $^{214}Po$.

The equilibrium-equivalent $^{222}Rn$ concentration (EERC) from each CR-39 was calculated theoretically by the equation 3-5. In this equation, $\eta$ is the collection efficiency of CR-39, that was estimated to be 11.84% for measuring the alpha particles emitted from aerosols and impinge on CR-39 through the proper Al film and 10.01% for measuring the alpha particles emitted from the surface of the glass fiber filter and impinge on the CR-39 through an air layer of 22.5 mm and the proper Al film.

In case of ELPI, the attached radon progeny was collected on the aluminum foil as a material substance at a flow rate of 29.4 $Lmin^{-1}$ for 5 minutes. After sampling, activity on the aluminum foil from stages $3^{rd}$ -$7^{th}$ (for 0.3 μm), $4^{th}$-$8^{th}$ (for 0.5 μm), $6^{th}$-$10^{th}$ (for 1 μm), were simultaneously measured using ZnS(Ag) scintillation detectors. The tests were also conducted with MOUDI to verify the size distribution of the developed technique with a diameter of 1 μm., Attached radon progeny were collected on the removable impaction plates in MOUDI, which used grease coating on each plate at a flow rate of 30 $Lmin^{-1}$ for 5 minutes. After sampling, activity on the removable impaction plates from stages $5^{rd}$ -$9^{th}$ (for 0.3 μm), $5^{th}$-$9^{th}$ (for 0.5 μm), $4^{th}$-$7^{th}$ (for 1 μm), were simultaneously measured with ZnS(Ag) scintillation detectors. The activity concentrations of radon progeny for ELPI and MOUDI at each stage were analyzed by using the decay method.

During the sampling period of ELPI, MOUDI and 4-stages impactor, a 400-mesh metal wire screen was set at the inlet of each sampler to prevent invasion of unattached progeny, and the collection efficiency was estimated to be 92.4%, 92.2%, and 99.9%, respectively based on fan model filtration theory. Two or Three air samples were taken under each condition.

Verification experimental results are shown in Table 4-11 and the example of activity size distribution of radon progeny from each impactor is shown in Figure 4-16.

To validate the developed technique with the commercial devices e.g. ELPI and MOUDI was conducted to obtain activity size distribution of radon progeny of particular particle size. Results have been given in Table 4-11 that the activity median aerodynamic diameters (AMAD) calculated by developed technique are corresponding with commercial devices from the range of 0.5 to 1 μm. However, AMAD from our technique was 43 % less effective than commercial devices at 0.3 μm. Due to our cut off diameter in last stages of impactor (0.5 μm) is bigger than 0.3 μm. In this case, the dose conversion factor was calculated using a dosimetric approach seemed to increase about 6% (Table 4-12). Moreover, the dose conversion factor of our technique at AMAD about 0.5 and 1 μm seemed to increase with $\sigma_g$ (Table 4-12) but less than 30%. Thus, for the measurements with particle size 0.3, 0.5 and 1 μm, this technique (4-stage impactor) was an alternative to ELPI and MOUDI from the viewpoint of dosimeter.

Table 4-11 Verification results of developed technique.

| Test ID | AMAD(μm) | | $\sigma_g$ | | Average AMAD (μm) | |
|---|---|---|---|---|---|---|
| | ELPI/MOUDI | 4-stage impactor | ELPI/MOUDI | 4-stage impactor | ELPI/MOUDI | 4-stage impactor |
| 0.3 μm; Test with ELPI/MOUDI | | | | | | |
| 1 | 0.312 | 0.440 | 1.35 | 1.91 | 0.302±0.013 | 0.431±0.013 |
| 2 | 0.292 | 0.422 | 1.35 | 1.89 | | |
| 0.5 μm; Test with ELPI(1,2)/MOUDI(3) | | | | | | |
| 1 | 0.496 | 0.542 | 1.36 | 1.96 | 0.453±0.043 | 0.495±0.064 |
| 2 | 0.451 | 0.520 | 1.36 | 1.91 | | |
| 3 | 0.411 | 0.422 | 1.43 | 2.01 | | |
| 1 μm; Test with ELPI(1-3)/MOUDI(4,5) | | | | | | |
| 1 | 0.995 | 0.942 | 1.29 | 1.77 | 1.076±0.083 | 1.035±0.089 |
| 2 | 1.168 | 1.073 | 1.43 | 1.81 | | |
| 3 | 0.982 | 0.938 | 1.32 | 1.94 | | |
| 4 | 1.108 | 1.125 | 1.46 | 1.93 | | |
| 5 | 1.125 | 1.099 | 1.46 | 2.07 | | |

Table 4-12 A comparison of dose conversion factor from dosimetric approach

| ELPI/MOUDI | | 4-stage impactor | | Dose conversion factor (nSv/(Bq h $m^{-3}$)) | | Difference value of dose (%) |
|---|---|---|---|---|---|---|
| Average AMAD (μm) | $\sigma_g$ | Average AMAD (μm) | $\sigma_g$ | ELPI/MOUDI | 4-stage impactor | |
| 0.302 | 1.35 | 0.431 | 1.90 | 9.41 | 9.93 | 6 |
| 0.453 | 1.38 | 0.495 | 1.96 | 7.82 | 10.12 | 26 |
| 1.076 | 1.39 | 1.035 | 1.90 | 14.73 | 16.43 | 11 |

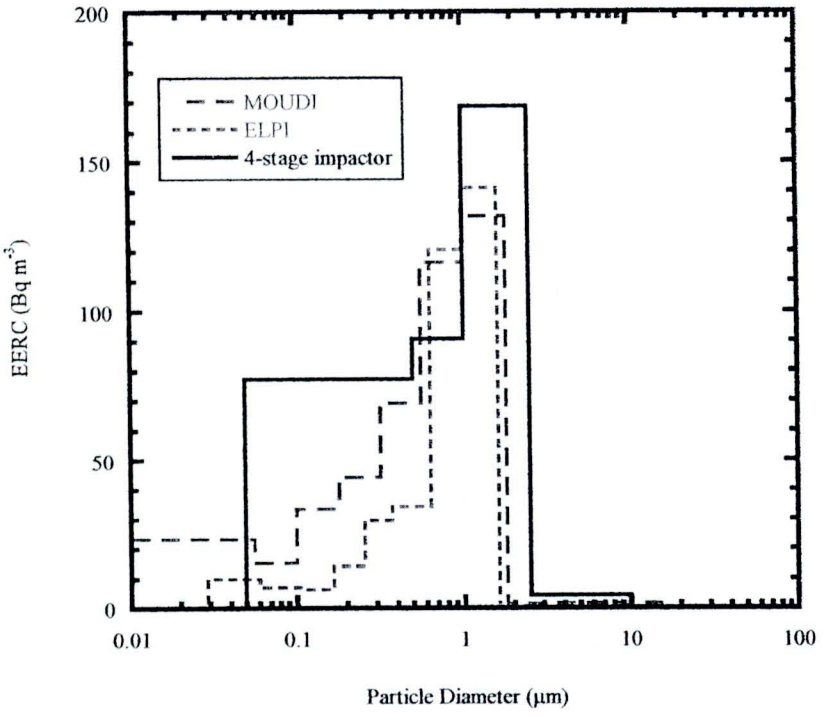


Figure 4-16 The activity size distribution of radon progeny: a) ELPI, b) MOUDI and c) 4-stage impactor. Sampling at radon concentration 5 $kBqm^{-3}$ and aerosol size 1 μm was generated.